CrystEngComm

Accepted Manuscript

ROYAL SOCIETY OF CHEMISTRY

www.rsc.org/crystengcomm

CrystEngComm

RSCPublishing

ARTICLE

Synthesis, X-ray characterization, DFT calculations and Hirshfeld surface analysis of M^{n+} ions (n = 2,3; M = Ni, Cd, Mn, Co and Cu): The role of secondary bonding and steric effects in complexes based on thiosemicarbazone

Cite this: DOI: 10.1039/x0xx00000x

Received 00th January 2012,
Accepted 00th January 2012

DOI: 10.1039/x0xx00000x

www.rsc.org/

Ghodrat Mahmoudi,[a]* Alfonso Castiñeiras,[b] Piotr Garczarek,[c] Antonio Bauzá,[d] Arnold Rheingold,[e] Vasyl Kinzhybalo[f] and Antonio Frontera[d]*

Two new pyridine-based heterocyclic thiosemicarbazone ligands and their Ni(II), Cd(II), Mn(II), Co(III) and Cu(II) complexes have been synthesized and characterized by structural, analytical and spectral methods. The mono-deprotonated anionic forms of the ligands coordinate in a tridentate fashion via two nitrogen and one sulphur donor atoms to yield seven complexes in which metal centres vary from four-coordinated square planar to six-coordinated distorted octahedral. Single-crystal X-ray crystallography showed that the molecular complexes can aggregate into larger entities depending upon the anion coordinated to the metal centre. We have analysed the interesting supramolecular assemblies observed in the solid state of some complexes by means of DFT calculations. These assemblies are formed by a combination of several noncovalent interactions, including chelate ring–π, π–π, and chalcogen bonding interactions that have been characterized using the Bader's Theory of "atoms-in-molecules".

1. Introduction.

The assembly of metal–organic polymers can be subtly influenced by various factors, such as solvent nature, molar ratio of reactants, reaction temperature, etc. Owing to their therapeutic potential, thiosemicarbazones constitute a class of ligand that presents a considerable interest to medicinal chemists.[1] Over the last few decades, thiosemicarbazones and their transition metal complexes have received substantial attention not only due to their valuable pharmacological properties, such as antibacterial, antitumor, antiviral and antimalarial activities but also their coordination behaviour.[2] These complexes can adopt different topologies, mainly monomers[3] and dimers.[4] The latter can be classified as S-bridged systems, whose metal ions are bridged through the thiosemicarbazone sulphur atom, and X-bridged systems where the non-thiosemicarbazone ligand acts as a bridge between the metal centres. Their participation in chain formation processes has also been reported.[5] We focused our work on the synthesis and crystallization of NON and NSN containing complexes.

Herein, we report the synthesis and characterization of a newly synthesized pyridine-based heterocyclic thiosemicarbazone ligand (see Scheme 1) and its mononuclear complexes with Ni(II), Cd(II), Mn(II), Co(III) and Cu(II), see Scheme 2. The syntheses were performed under mild solvothermal conditions in an interesting and unusual glassware apparatus that has been recently developed by us.

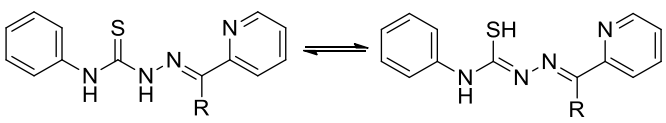

HL_1; R=H
HL_2; R=CH_3

Scheme 1 Molecular diagrams of HL_1 and HL_2.

The theoretical study reported herein is devoted to the analysis of the supramolecular assemblies observed in the solid state, evaluating the different contributions to molecular recognition and to assign discrete energy values to them. By means of high level DFT calculations and using several theoretical models we have studied these energetic contributions in the solid state crystal structures that are useful for the understanding of the noncovalent forces and for rationalizing their influence in the

crystal packing paying attention to the more unconventional (less studied) interactions. For instance, in the Ni compounds **1** and **2** we have analysed the antiparallel chelate ring π–interactions. The conventional π–stacking interactions[6] usually comprise organic aromatic molecules. However, other planar molecules and fragments can also be involved in "non conventional" stacking interactions[6a,7]. For instance, in transition-metal complexes planar chelate rings with delocalized π-bonds can establish stacking7 interactions, which are similar to those of organic molecules.6 In fact, π-stacking interactions between chelate and aromatic rings in crystal structures of square-planar transition-metal complexes7 have been analysed, showing preference for the offset face-to-face orientation. In compound **3** we have analysed the formation of electrostatically enhanced $\pi^{\delta+}$–$\pi^{\delta-}$ interactions in the solid state and, finally, in compounds **4** and **7** we have studied the relevant chalcogen (N···S) interactions between the azide ligand and the sulfur atom of the ligand.

2. Experimental.

2.1. Materials and methods

The ligands HL_1 and HL_2 were prepared[8] following the method described below and used without further purification. All other reagents and solvents used for the synthesis and analysis were commercially available and used as received. FT-IR spectra were recorded on a Bruker Tensor 27 FT-IR spectrometer. Microanalyses were performed using a Heraeus CHN-O-Rapid analyzer.

2.2. Synthesis of HL_1 and HL_2

4-phenyl-3-thiosemicarbazide (1.67 g, 10 mmol) was dissolved in 100 ml of anhydrous methanol, then 1 ml (10 mmol) of freshly distilled 2-pyridinecarboxaldehyde and a drop of conc. HCl were added and the mixture was heated to reflux for 2 h. Next it was slowly cooled to room temperature to yield crystalline solid, which was filtered off and dried in air. HL_2 was prepared using the same procedure as HL_1 except 2-acetyl pyridine was used.

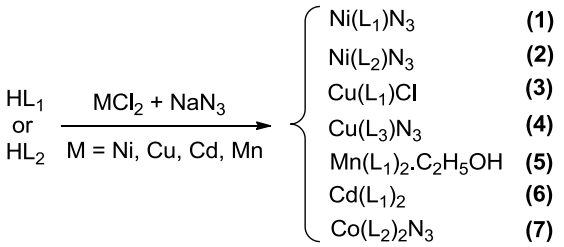

Scheme 2. Compounds **1–7** reported in this work. See below for the definition of L_3.

2.3. Synthesis of complexes

The complex **1** was synthesized in a reaction of organic ligand, HL_1, (0.026 g, 0.10 mmol) with $NiCl_2$ (0.01 g, 0.10 mmol) and sodium azide (0.065 g, 1.0 mmol) using a thermal gradient method in a branched tube with ethanol (10 ml) as solvent. The tube was sealed and immersed in an oil bath at 60 °C while the branched arm was kept at ambient temperature. After 2 days, crystals of **1** formed in the cooler arm and were filtered off, washed with acetone and ether, and dried in air. Crystals of **2** were prepared by a similar synthetic procedure, except HL_1 was replaced by HL_2. $NiCl_2$ was replaced by $CuCl_2.2H_2O$ to for **3** and **4**. $CoCl_2.6H_2O$ was used for 7 and $MnCl_2.4H_2O$ or $CdCl_2$ for **5** and **6** respectively in a similar synthetic procedure.

For **1**: (0.03 g, yield 81%), found; (C, 43.68; H, 3.13; N, 27.67%. calcd. for $C_{13}H_{11}N_7NiS$; C, 43.76 H, 3.11; N, 27.54%) IR (cm^{-1}) selected bands: 747 ν(C=S asym), 1539 ν(C=S), 1599 ν(C=N), 2153 ν (N=N).

For **2**: (0.03 g, yield 80%), found; (C, 45.68; H, 3.43; N, 26.67%. calcd. for $C_{14}H_{13}N_7NiS$; C, 45.44 H,3.54; N, 26.50%) IR (cm^{-1}) selected bands: 746 ν(C=S asym), 1542 ν(C=S), 1597 ν(C=N), 2063 ν(N=N).

For **3**: (0.03 g, yield 85%), found; (C, 44.18; H ,3.23; N, 15.67%. calcd. for $C_{13}H_{11}ClCuN_4S$; C, 44.07 H,3.13; N, 15.81%) IR (cm−1) selected bands: 754 ν(C=S asym), 1542 ν(C=S), 1601 ν(C=N).

For **4**: (0.03 g, yield 88%), found; (C, 44.78; H, 3.43; N, 16.87%. calcd. for $C_{14}H_{13}CuN_7S$; C, 44.85 H, 3.50; N, 16.95%) IR (cm^{-1}) selected bands: 574(w), 694(s), 780(s), 1003(w), 1159(m), 1250(w), 1437(m), 1576(s), 1612(s), 3060(w).

For **5**: (0.03 g, yield 85%), found; (C, 50.46; H, 4.71; N, 15.77%. calcd. for $C_{15}H_{17}MnN_4OS$; C, 50.56 H, 4.81; N, 15.72%) IR (cm^{-1}) selected bands: 566(w), 692(s), 778(m), 1010(w), 1157(m), 1250(w), 1435(m), 1592(m), 1620(s), 3059(w).

For **6**: (0.03 g, yield 75%), found; (C, 42.16; H, 3.71; N, 14.17%. calcd. for $C_{14}H_{15}CdN_4OS$; C, 42.06 H, 3.78; N, 14.01%) IR (cm^{-1}) selected bands: 576(w), 690(s), 770(m), 1017(w), 1150(m), 1250(w), 1435(m), 1582(m), 1610(s), 3050(w).

For **7**: (0.04 g, yield 65%), found; (C, 51.16; H, 3.71; N, 25.27%. calcd. for $C_{28}H_{26}CoN_{11}S_2$; C, 51.06 H, 3.63; N, 25.19%) IR (cm^{-1}) selected bands: 694(s), 756(m), 1110(w), 1164(m), 1254(w), 1432(s), 1601(m), 2007(s), 2928(w).

2.5. X-ray crystallography

The diffraction data were collected on Kuma KM4CCD (**1**, 295 K, λ = 0.71073 Å), Bruker APEX II (**2** , 100 K, λ = 0.71073 Å), Bruker X8 Proteum (**3**, 296 K, λ = 1.54178 Å) and Oxford Diffraction Xcalibur Kappa CCD (**4** - **7**, 295 K, λ = 0.71073 Å) X-ray diffractometers. Data were processed with Apex2 (**2**, **3**)[9] and CrysAlisPro (**1**, **4** - **7**)[10] programs and corrected for absorption using SADABS[11] The structures were solved by direct methods,[12] which revealed the position of all non-hydrogen atoms. These atoms were refined on F^2 by a full-matrix least-squares procedure using anisotropic displacement parameters.[12] All hydrogen atoms were located in difference Fourier maps and included as fixed contributions riding on attached atoms with isotropic thermal displacement parameters 1.2 times those of the respective atom. All calculations were performed and the drawings were prepared using WINGX crystallographic suite of programs.[13] The crystal data are listed

in Table S1. Crystal structure visualizations were prepared using Diamond.[14] Further details are available from the Cambridge Crystallographic Centre with quotation numbers 1046009-1046016.

2.6. Theoretical methods

The geometries of the complexes included in this study were computed at the BP86-D3/def2-TZVP level of theory using the crystallographic coordinates within the TURBOMOLE program.[15] This level of theory that includes the latest available dispersion correction (D3) is adequate for studying non covalent interactions dominated by dispersion effects like π-stacking. The basis set superposition error for the calculation of interaction energies has been corrected using the counterpoise method.[16] The "atoms-in-molecules" (AIM)[17] analysis of the electron density has been performed at the same level of theory using the AIMAll program.[18] The Molecular Electrostatic Potential (MEP) surfaces have been computed at the B3LYP/6-31+G* level of theory since this level has been successfully used before to analyse similar systems.[19]

2.7 Hirshfeld surface

Hirshfeld surface and 2D fingerprint calculations were performed using the CrystalExplorer package ver. 3.1.[20] Crystal structures were imported from CIF files. Hirshfeld surfaces were generated for complex molecules using high resolution and mapped with the d_{norm} or shape index functions. 2D fingerprint plots were prepared with the use of the same software.

3. Results and discussion

3.1. Crystal structures of 1–7

Single crystal X-ray diffraction studies of all seven coordination compounds **1**–**7** were made. All the bond lengths and angles in the ligands have the usual values for coordinated NNS tridentate thiosemicarbazones. The N-N distances in all complexes [av. 1.374 Å] are very close to the distance found in the uncoordinated ligands (1.375 Å for L_2). By contrast, coordination lengthens the C-S bond of the metallacycles [av. 1.746 Å, 1.671 Å (L_2)] and the exocyclic C-N bond [av. 1.291 Å, 1.291 Å (L_2)] shortens the C-N bond of the metallacycles [av. 1.316 Å, 1.361 Å (L_2)]. These changes may be ascribed to the deprotonation of the ligands: the thiolization and the loss of the proton originally bound to N produce a negative charge which is delocalized in thiosemicarbazone moiety.[8]

$[Ni(L_1)N_3]$ (1) and $[Ni(L_2)N_3]$ (2)

The molecular structures of $[Ni(L_1)N_3]$ (**1**) and $[Ni(L_2)N_3]$ (**2**) are shown in Fig. 1, and selected bond lengths and bond angles are summarized in Table S2. In both compounds the ligand is deprotonated, each nickel(II) coordinates to the pyridine (N_{py}) and azomethine (N_{azm}) nitrogen atoms and the thiolato sulfur atom, finally, an N atom of azido ion (N_{az}) fulfils the metal coordination sphere. The four donor atoms are almost coplanar, and the metal atom lies just 0.01 Å for **1** and 0.03 Å for **2**, from the main ligand plane, although tetragonal distortions appear in the S-Ni-N_{py} and N_{azm}-Ni-N_{az} angles [170.10(5)° and 176.50(2)° in **1** as well as 170.13(7)° and 175.72(11)° in **2**]. Comparison of Ni-N_{py} and Ni-N_{azm} distances [1.925(2) versus 1.846(2) Å in complex **1**, 1.932(2) versus 1.850(2) Å in complex **2**] shows that the bond with the azomethine nitrogen atom is stronger, obviously due to the greater basicity of this nitrogen atom. The azido ligand is quasi-linear; the N1N-N2N-N3N bond angle is 175.7(2)° for **1** and 175.4(3)° for **2**, showing asymmetric N-N distances of 1.196(2)/1.150(2) Å for **1** and 1.201(3)/1.151(3) Å for **2**. The Ni-N1N-N2N angle are 124.3(2)° and 125.4(2)° for **1** and **2**, respectively. The Ni-S and Ni-N_{az} distances are similar to those found in other complexes in which Ni coordinates to S or N_{az}.[21] The delocalization of the charge originated by deprotonation at hydrazine nitrogen atom (N_{hz}) is apparent upon comparison of the thiosemicarbazones bond lengths in the complexes and the free ligand. In both complexes N_{hz}-C is shorter and C-S is longer than in free HL_1 or HL_2,[8,22] thus, bond order is increased in the former case and decreased in the latter, as observed for similar complexes. The stability of complexes **1** and **2** is increased by the rigidity of the planar tricyclic system formed by the pyridine ring and the two five-membered chelation rings.

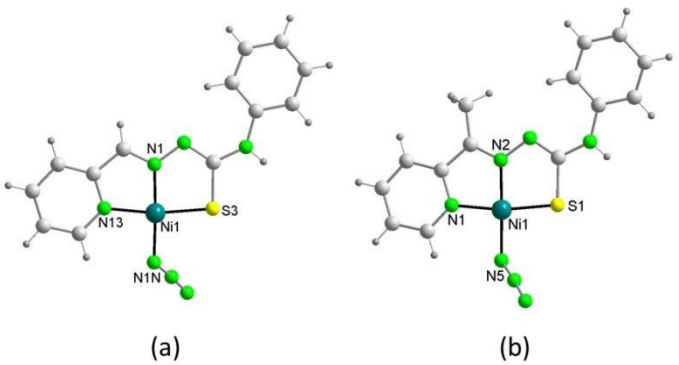

Fig. 1. Perspective view of the molecular structures of: a) $[Ni(L_1)N_3]$ and b) $[Ni(L_2)N_3]$.

Analysis of the molecular packing in **1** and **2** shows intermolecular hydrogen bonding interactions that exclusively consist of classical N–H···N bonds (see Fig. S1 and Table S3). The intermolecular complexes are organized in pairs step-shaped involving mutually *syn* thioamine N_{ta}–H and terminal azide nitrogen atoms, N_{az}, in an end-to-end azido bridges fashion, thus forming $R_2^2(16)$ rings (Fig. S1). In addition, the metal-chelate rings Cg(1) [Ni1/S3/C3/N2/N1] and Cg(2) [Ni1/N1/C11/C12/N13] establish π-π interactions involving metal-chelate rings of neighbouring molecules at an average distance along *a* axis of 3.535(2) Å in **1**, resulting in a three-dimensional network (Fig. S2, Table S4). In addition, the pyridyl ring Cg(3) [N1/C1/C2/C3/C4/C5] also participates in these interactions at an average distance of 3.576(2) Å in **2**, with the formation of infinite one-dimensional chains mutually perpendicular (Fig. S3, Table S4).[23]

$[Cu(L_1)(\mu\text{-}Cl)]_2.[Cu(L_1)(Cl)]_2$ (3)

Complex **3** crystallizes in the monoclinic $P2_1/n$ space group consisting of a cocrystal of dinuclear metallacycle and mononuclear complex molecules (Fig. 2). The asymmetric unit contains one-half of the metallacycle unit, and one mononuclear complex. Significant structural parameters are given in Table S1. The structure of the mononuclear molecule (Fig. 2a) shows that the mononegative thiosemicarbazone ligand (L_1) binds to the Cu(II) center via N,N,S-donor atoms, resulting in two five membered chelate rings. The fourth coordination site around Cu(II) is occupied by a chloride, forming a distorted square planar complex. It is also worth stressing that the bonding parameters are in good agreement with the coordinating pattern of a thiosemicarbazone via the thiolate form. While coordinated in their iminothiolate forms, the negative charges generated by deprotonation are effectively delocalized in the C–N–N–C system, as shown by the intermediate C8–N3 [1.285(3) Å], N3–N2 [1.371(3) Å] and N2–C7 [1.320(3) Å] bond distances. The bond angles Cl1–Cu1–S1 98.36(3)°, Cl1–Cu1–N4 97.32(7)°, N3–Cu1–S1 83.43(7)° and N3–Cu1–N4 80.93(9)° illustrate that the complex is slightly distorted from the square planar geometry (τ_4 = 0.13).[24]

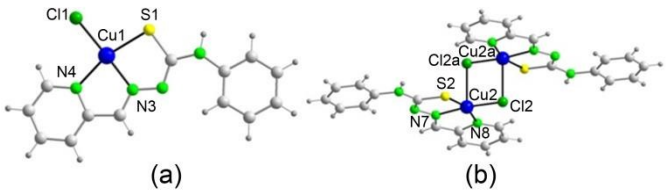

Fig. 2. Perspective view of the cocrystal of: a) mononuclear and b) dinuclear metallacycle complex molecules, of compound $[Cu(L_1)(\mu\text{-}Cl)]_2{\cdot}[Cu(L_1)(Cl)]$.

In the centrosymmetric metallacycle (Fig. 2b) the Cu(II) ion is presented in a distorted square pyramidal as evidenced from the trigonality index value, τ = 0.19.[25] The L_1 ligand coordinates meridionally to the central Cu(II) ion, as commonly observed for other reported complexes involving thiosemicarbazones.[26] Three coordination positions are occupied by the pyridine nitrogen N8, imine nitrogen N7 and the thioether sulfur S2 atoms, respectively. The remaining one is occupied by a chloride ion, namely Cl2 which bridges two mononuclear complexes, thus forming a metallacycle (Fig. 2b). The symmetry generated Cl2[a] (a: 2-x, -y, 2-z) is situated at the apex of the square pyramidal structure. The equatorial Cu–Cl distance is much shorter [2.2535(7) Å] than the axial Cu–Cl distances [2.8140(1) Å]. The Cu(II) ion is located at 0.102 Å out of plane towards the axial chloride atom. X-ray structure analysis clearly reveals that two square pyramids symmetrically related are fused together at the base-to-apex edge. The Cu–Cl distances of 2.2535(7) Å and 2.8140(1) Å and the Cu–Cl–Cu angle of 85.36(2)° are fairly consistent with the corresponding Cu–Cl distances and the Cu–Cl–Cu angles of the similar bis-μ-chloro-bridged dicopper(II) complexes with a supporting tridentate ligand.[27] The existence of an inversion center influences the planarity of the central Cu_2Cl_2 moiety. The Cu-Cu distance is 3.4598(1) Å , which is too long to represent any bonding interaction, in agreement with their d^9 electronic configuration.

It is also remarkable the presence of classical and non-classical hydrogen bonding, π-π stacking and ring-metal interactions, that clearly govern the crystal packing formation (Fig. S4). Each ligand molecule of the dinuclear compound is interlinked to a ligand molecule of the mononuclear one via strong self-complementary hydrogen bonds N-H···S (2.77 Å, Table S3), giving rise to a $R_2^2(8)$ motif. In addition to these hydrogen bonds, two additional hydrogen bonds C-H···S (av. 2.945 Å) and four non-classical hydrogen bonds C-H···Cl (av. 2.865 Å) were also found with graph set motifs $R_2^2(8)$, $R_2^1(6)$ and $R_2^1(4)$ (Fig. S4a). These six hydrogen bonds help the lattice to grow along the *b* and *c* axes. The square pyramidal and square planar geometries of both copper(II) centres require that each CuL_1 to adopt a planar conformation. The two crystallographically independent CuL_1s are almost planar in both compounds. It is worth noting that some axial positions of each copper(II) are not occupied; however, the structural analysis showed that the planar CuL_1s are arranged in layers perpendicular to the *a* axis within the range of 3.280 to 3.8 Å, similar to a classical π-π stacking interaction.[23] In the present compound, this stacking arrangement involves three ring-ring interactions between the pyridine and phenyl rings, and four ring-metal chelate interactions involving phenyl rings (Fig. S4b). The average distance between rings is 3.701(2) Å, while the average ring-metal chelate distance is 3.568(2) Å. Three metal···π aryl weak intermolecular interactions[28] between the copper(II) ions and the phenyl rings of the thiosemicarbazones ligands are observed (Fig. S4c), where the distance between the centroids of the phenyl rings and the copper atom are less than 4.0 Å and the angle defined by the vector perpendicular to the aromatic ring and the vector passing through the centroid to the copper atom are less than 40° (Table S4). Thus, as shown in Fig. S4d and Table S4, the thick layers of the 2D metal complexes are packed through metal-organic ring interactions forming a 3D-supramolecular architecture.

$[Cu(L_3)\mu\text{-}N_3]_2$ (4)

A perspective view of the complex is displayed in Figure 3 and crystal data and selected bond parameters are listed in Table S2. The structure contains a five-coordinated centrosymmetric dicopper complex, where the two Cu(II) ions are bridged by two azides. The bridging azides are end-on coordinated. Each Cu(II) in the dicopper core is further bound by the monodeprotonated L_3 ligand coming from an unusual cyclization of the thiosemicarbazone HL_2 catalyzed by Cu(II) (see Scheme 3).[29] Each benzothiazolato ligand acts as a tridentate chelate, coordinating by the pyridyl nitrogen (N4), azometine nitrogen (N3) and the benzothiazole nitrogen (N1) thus materializing a quasi-square pyramid. The base of each distorted square pyramidal unit is occupied by N1, N3, N4 and N5[a] atoms (a: -x, 2-y, -z), with the apical position occupied by the N5 atom of the second azido ligand (Cu-N5, 2.376(1) Å). The average Cu-N bond length in the basal plane is 1.9946 Å, involving the azomethine and azido symmetry related nitrogen

atoms, closer to the Cu-N distance in pyridine and benzothiazole compounds. A maximum deviation of 0.1603 Å at N3 is revealed at the base of the square-pyramid with the central Cu(II) atom positioned 0.0169 Å above the mean plane. The pyridyl ring is less deviated from the basal plane (the dihedral angle between the two least square planes is 8.00°), when compared to the thiosemicarbazone moiety, which deviates more, at a dihedral angle of 11.86° from the basal CuN_4 plane. Due to the presence of an inversion center in the dimer, the bridging Cu_2N_2 network is perfectly planar and the Cu1-N_{az}-Cu1[a] bond angle is 82.97(6)°, smaller than the range of published Cu-azide-Cu angles in azide-bridged polynuclear compounds.[30] The end-on azide bridge is essentially linear with a N5-N6-N7 angle of 177.04(18)° and shows asymmetric N-N distances of 1.205(2) and 1.154(2) Å. Two neighbouring bridged Cu^{2+} ions form a binuclear unit in which the bond lengths of Cu1-N5 are 1.9600(14) and 2.3761(15) Å. The Cu1···Cu1[a] and N5···N5[a] separations in the dimer are 3.260(1) and 2.889(1) Å, respectively. These values lie in the typical range for double end-on azido-bridging copper(II) complexes.[31]

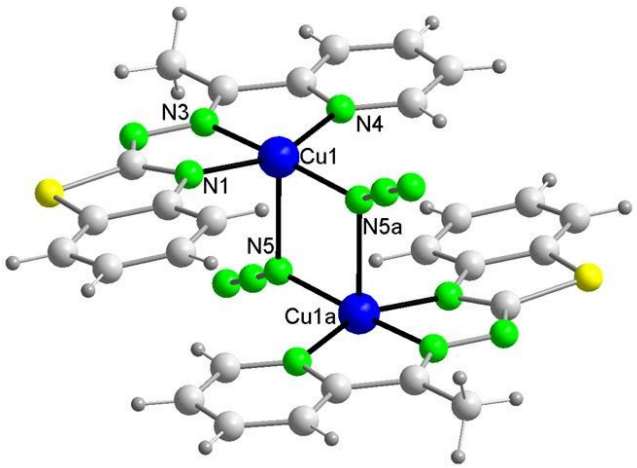

Fig. 3. Perspective view of the dimer $[Cu(L_3)\mu\text{-}N_3]_2$.

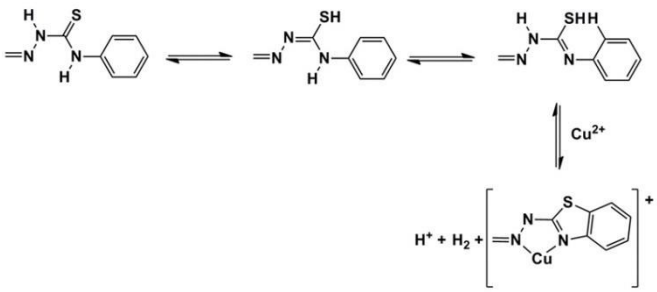

Scheme 3. Proposed mechanism for the cyclization of N-phenyl-thiosemicarbazones to benzothiazolato.

The bond distances and bond angles for the benzothiazolato ring are in good agreement with the expected values.[32] Comparison of the structures of benzothiazole ligand with that of the starting thiosemicarbazone HL_2, show that the cyclization and complexation decrease the length of N2-N3 and C1-N2 bonds, but the N1-C1 length remains unchanged with respect to the thiosemiarbazone due to a significant increase in the partial double bond character.8 The angle that is changed the most is N1-C1-S1 which decreases by about 10º from the HL_2 due to the tension of the pentacycle upon complexation.

In the crystal structure of **4**, classical hydrogen bonds are not present, but the presence of a C-H···S link between C14 and S1 of the adjacent dinuclear (b: -x, y+1/2, -z+1/2) is remarkable. In the complex, the H···S distances is 2.99 Å and the C14-H14B···S1 angle is 149.7°; the values suggest strong interactions in the complex with this non classical noncovalent contacts (Table S3, Fig. S5a). In addition, π-π stacking interactions are observed between the thiazole rings and the pyridyl rings from the adjacent molecules, and vice versa, with centroid-centroid distances of 3.822(1) Å (Table S4, Fig. S5b). Intermolecular interactions between the phenyl ring and the copper atom link the molecules into an infinite three-dimensional network (Fig. S5c). The Cu···centroid distance is 3.822(1) Å, while the distance of the copper atom to the nearest C atom of the phenyl ring is 3.075(1) Å.

$[Mn(L_1)_2]\cdot EtOH$ (5) and $[Cd(L_1)_2]\cdot MeOH$ (6)

Figure 4 shows the molecular structures of compounds **5** and **6**, and Table S2 lists their main bond lengths and angles. They have isotypic structures and also with $[Cd(L_1)_2]\cdot CH_3CN$,[33] both being distorted octahedral complexes in which the metal atom is hexacoordinated to the pyridyl nitrogen, N(1), the azomethine nitrogen, N(2), and the thiolato sulfur atoms of two monodeprotonated L_1 ligands in a *trans*-N(2)–*cis*-N(1)–*cis*-S configuration. In any case the disposition of these ligands drives to the formation of *mer* type isomers. Both structures contain a crystallographic twofold axis bisecting the S-M-S and N1-M-N1 angles. The bond lengths M-N_{azm} are shorter than the M-N_{py} ones, and, as expected, the M-S bonds are longer than the M-N bonds, making the coordination figure distorted. In **5** the Mn-S distance, 2.5092(6) Å, is similar to those found in other hexacoordinate complexes of manganese(II) with monodeprotonated thiosemicarbazones,[34] and the Mn-N distance, av. 2.256(2) Å, is also in the range found in thiosemicarbazonates of Mn(II).[35] In **6**, the Cd-S distance, av. 2.5675(2) Å, is in the usual range for hexacoordinate Cd(II) complexes,[36] and the Cd-N distance, av. 2.374(3) Å, is likewise similar to those of other complexes of cadmium(II) with thiosemicarbazones.[36] As in other metal thiocarbazonate complexes and in complexes **1**-**4**, the negative charge of the monoanionic ligand is delocalized over the L_1 moiety and the S–C bond distance is consistent with increased single bond character, while both distances C-N, imine and thioamide, indicate significant double bond character. The S–M–S angle is much greater than 90º in both complexes [96.80(3)º in **5** and 100.78(6)º in **6**] and demonstrates that the two ligands exert significant steric effects on each other. The tridentate ligand is nearly planar. The displacement from coplanarity is indicated by the dihedral angle between the pyridyl ring and the plane defined by the five-membered chelate ring M–S–C–N–N, and between the pyridyl ring and the plane defined by M–N–C–C–

N of 6.29(3) and 3.44(4)º, and 6.22(4) and 3.72(4)º, for **5** and **6**, respectively.

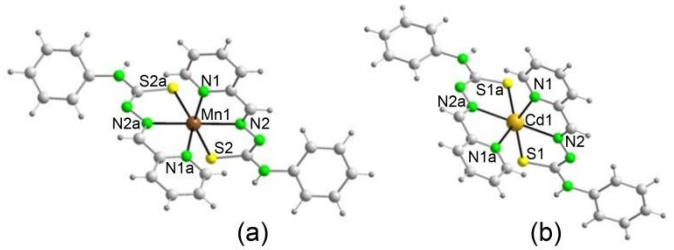

Fig. 4. Perspective view of the molecules of: a) $[Mn(L_1)_2]$ and b) $[Cd(L_1)_2]$.

The crystal packing features of compounds **5** and **6** have been analysed as a whole due to their clear similarities in their solid state architecture (Figs. S6 and S7, respectively). The polar hydrogen atom on N_{ta} participates in intermolecular hydrogen bond (Table S3). Each molecule of complex form hydrogen-bonded dimers linked by two weak N_{ta}–H···S hydrogen bonds involving the thioamide hydrogen atom and the adjacent sulfur atom and vice versa of centro-symmetrically related pairs of molecules through heterosynthons of $R_2^2(8)$ motif (Figs. S6a and S7a), results in the formation of infinite one-dimensional chains in the direction of *c* axis. Intramolecular hydrogen bond stabilizes the structure, while the crystal packing is determined by intermolecular hydrogen bonds and π-π interactions. The most significant stacking interactions involve the pair of pyridine rings at a centroid to centroid separation of 3.784(1) and 3.647(2) Å, for **5** and **6**, respectively (Figs. S6b and S7b). In addition, in **5** and **6** we also appreciate the existence of stacking interactions of between its pyridine ring and the corresponding metal-(pyridine-azomethine nitrogen atoms) chelate rings with centroid-centroid distances of 3.769(2) and 3.785(2) Å, respectively (see Table S4 and Figs. S6b and S7b) forming infinite one-dimensional chains in the direction of *a* axis. On the other hand, data of Table S3 reveal that both compounds display a weak non classical intermolecular C-H···S interaction, reinforcing the chains formed in the direction of *a* axis. Finally, although the packing of manganese complex has similar characteristics than resemble the cadmium complex, in the crystal lattice of **5** some C-H···π interactions between phenyl ring and manganese chelate rings are observed (Table S4).

$[Co(L_2)_2](N_3)$ (7)

The molecular structure of **7** consists of mononuclear cobalt(III) cationic units (Fig. 5) and uncoordinated azide N_3^- anions. The metal centers in the complex possess an octahedral geometry with two deprotonated ligands. The Co(III) ion is coordinated in a meridional fashion using pairs of *cis* pyridyl nitrogen, *trans* azomethine nitrogen and *cis* thiolate sulfur atoms from two monoanionic ligands. This coordination results in four five-membered chelate rings in thecomplex. The bond angles suggest distorted octahedral coordination geometry in the complex. The dihedral angle formed by the mean planes of the bicyclic chelate systems of each of the ligands is 88.085(13)°. Each bicyclic chelate system, Co1/S1/C8/N3/N2/C6/C5/N1 and Co1/S2/C22/N7/N6/C20/C19/N5, are approximately planar as evidenced by the maximum deviation of 0.034(7) Å for N1 and 0.030(7) Å for C22, respectively. In **5**, the bicyclic chelate system Mn1/S2/C7/N3/N2/C6/C5/N1 is approximately planar with a maximum deviation of 0.072(7) Å for C5, while in **6** the corresponding bicyclic Cd1/S1/C7/N3/N2/C6/C5/N1 show a maximum deviation of 0.088(5) Å for S1. These results suggest the distortion in the octahedral geometry is less in **7**, compared to **5**, and in this one, compared to **6**. On complexation the ligand HL_2 undergoes structural reorientation to coordinate the metal in a NNS manner.

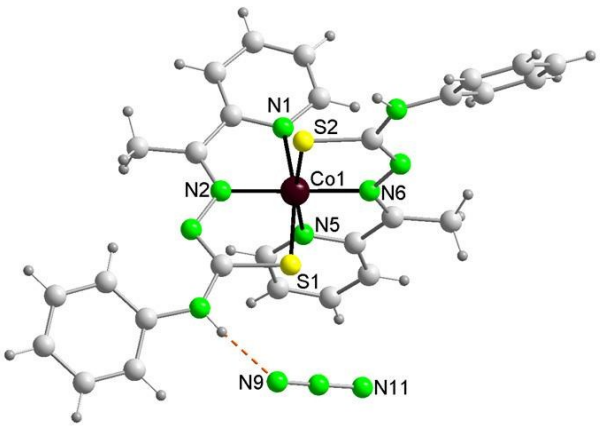

Fig. 5. Perspective view of the molecular structure of $[Co(L_2)_2](N_3)$ with cation-anion hydrogen bonds.

The free thiosemicarbazone crystallizes in the *EE* conformation.8 A twisting of approximately 180° in the N3–C8 and N7-C22 bonds of the thiosemicarbazone to match the steric requirements of tridentate coordination was evidenced. Therefore, in complex the ligand adopts the *EZ* conformation. Hence some angles undergo significant changes on complexation. The C8–N3–N2 angle goes from 118.89° in HL_2 to 111.1(3)° and 112.2(3)° in the complex; N3–C8–S1 goes from 119.68° in HL_2, to 124.7(3)° and 124.2(3)° in cobalt(III) complex. There is a slight shortening of the bond distance between Co and the imine nitrogen [1.880(3) and 1.888(3) Å] compared to the distance between Co and the hetero-aromatic nitrogen [1.969(3) and 1.955(3) Å], indicating the greater strength of former bonds compared to the latter. Similar feature was observed in the Mn(II) and Cd(II) complexes. The Co–S and Co–N bond lengths in both complexes are comparable to those with other cobalt(III) tiosemicarbazonates.[37] The C–S bond length increases to 1.744(4) Å [C8–S1] and 1.748(4) Å [C22–S2] from 1.6849(13) Å in HL_2.8 The N3–C8 bond length also changes from 1.3587(16) Å to 1.316(4) Å [1.305(4) Å for N7–C22] due to enolization of the ligand for coordination after deprotonation.

An analysis of the crystal packing reveals that the azide anion is engaged in strong classical hydrogen bonding [N4···N9, 2.914

Å and N8···N11[a], 2.950 Å (a: x, -y+1/2, z+1/2)] with the thioamide-NH fragments of the ligands, stabilizing the thione form of the ligands (Fig. S8). Each cation complex binds to two azide anions (Fig. S8a) while each azide anion binds to two cation complexes (Fig. S8b). Thus, the azide anions act as bridge between cations to build infinite one-dimensional chains along the *c* axis (Fig. S8c). In addition, nonclassical weak intramolecular interactions are observed between the metal chelate rings and C1 and C15 atoms of pyridine rings (av. C···Cg, 2.887 Å) that stabilize the molecular structure (Fig. S8d).

Hirshfeld surface analysis

Hirshfeld surface based tools represent a unique approach to the crystal structure prediction and this method offers a facile way of obtaining information on trends in crystal packing.[38] The derivation of Hirshfeld surface and breakdown of the corresponding 2D fingerprint plot provide a convenient means of quantifying the interactions within the crystal structures, revealing significant similarities and differences between related structures by individuating the packing motifs.

Compounds 1 and 2

Hirshfeld surface (HS) of compounds **1** and **2** bear a lot of similarities (due to similar structure of the complex compounds) and will be therefore described together. On the surface of both compounds mapped with d_{norm} function one can notice two big red areas as well as two smaller ones next to them (Fig. 6). They are consistent with strong hydrogen bonds mentioned in the crystal structure (N4-H4···N3N and N4-H1N···N7 for **1** and **2**, respectively) and weaker ones (C10-H10···N3N and C10-H10···N7, respectively). Additionally in the case of compound **1** two small red areas correspond to close H···H contact (2.11 Å) can be seen (consistent with the spike on the decomposed fingerprint plot – Fig. S10a). In compound **2** the close H···H contact is also present (as indicated by a spike on decomposed fingerprint plot – Fig. S11a) however the distance (2.2 Å) makes it not appear on the surface as a red spot. Biggest differences between surfaces of the compounds are connected with sulphur atom contacts. In compound **1** close contact between C11 of one molecule and S3 of an adjacent molecule is visible on the HS as two small red areas. In case of compound **2** presence of a methyl group (instead of a proton) facilitates formation of an additional weak C-H···S hydrogen bond (C7-H7B···S1) which is represented on HS as two small red areas.

When shape index function is applied to the Hirshfeld surface "bow-tie" patterns can clearly be seen indicating π···π stacking interactions. In **1** stacking interactions are present between phenyl and pyridyl rings as well as "coordination rings" of adjacent molecules. Presence of a light region in the decomposed C···C fingerprint plot (Fig. S10d) further confirms existence of aromatic ring stacking interactions. In case of **2** stacking interactions, which are visible as 'bow-tie' patterns marked on Fig. S9b, occur between pyridyl and coordination rings of adjacent molecules. Study of decomposed fingerprint plots (Fig. S10 and S11) shows that most important interactions between molecules in crystals of **1** and **2** are van der Waals forces (32.5% and 33.9% respectively), strong N-H···N hydrogen bonds (24.6% and 25.5%) and C-H···C and C-H···π interactions (15.5% and 14.2%).

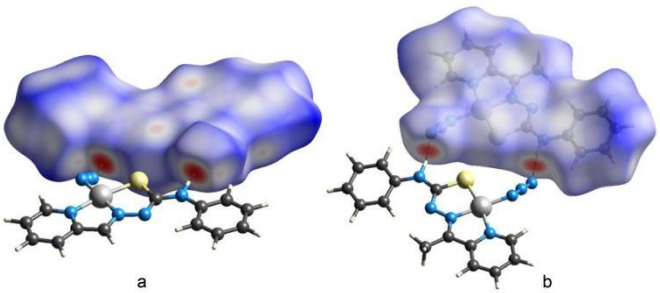

Fig. 6. Hirshfeld surface of **1** (a) and **2** (b) mapped with d_{norm} function. N-H···N hydrogen bonds marked as dashed lines.

Compound 3

For compound **3** the asymmetric unit was used for Hirshfeld surface calculations. Therefore the long Cu-Cl (apical) bonds are represented as two big red areas on the 'top' of the surface mapped with d_{norm} function. There are four more large red areas on the 'rant' of the HS which correspond to two N-H···S hydrogen (N5-H5···S1 and N1-H1···S2, Fig. 7) which are responsible for formation of a supramolecular chain.

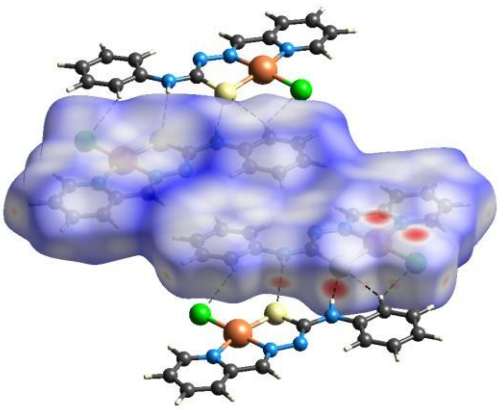

Fig. 7. Hirshfeld surface of **3** mapped with d_{norm} function. Hydrogen bonds marked with dashed lines.

Additionally several smaller red spots are visible on the 'edge' of the surface which represent four weak C-H···X (X = S, Cl) hydrogen bonds, namely C2-H2···S2, C12-H12···Cl2, C25-H25···Cl1 and C2-H2···Cl2. Moreover there are weak hydrogen bonds which are too long to show up on the surface mapped with d_{norm} (C15-H15···S1 and C15-H15···Cl1). Last four red spots present on the 'edge' of the surface come from short H···H contacts - H25···H16 (2.093Å) and H3···H12 (2.114 Å). All of the mentioned hydrogen bonding is responsible for formation of a supramolecular layer. Connection between the layers is achieved by phenyl and pirydyl as well as coordination rings interactions. Stacking

interactions show up on the d_{norm} mapped surface as six red areas representing four C···C contacts, which is consistent with a bright area on the decomposed fingerprint plot (Fig. S13d).
Shape index function is more suitable for analysis of such interactions. On the 'bottom' part of the Hirshfeld surface several 'bow-tie' patterns can be seen (marked on Fig. S12) which indicate stacking interactions between phenyl rings of molecules in one layer and pirydyl rings of molecules of adjacent layer. Analysis of the decomposed fingerprint plots (Fig. S13) indicates that the most important types of interactions in the crystal packing of **3** are van der Waals forces (27.9%), medium and weak hydrogen bonds (H···S and H···Cl contacts make 28.4% of the surface) and stacking interactions.

Compound 4

Examination of the Hirshfeld surface of compound **4** mapped with d_{norm} function (Fig. S14) reveals only four red areas. Surprisingly they do not correspond to any hydrogen bonds, but to short N···S contact (N7···S1). Long, weak C-H···X (X=N, S) H bonds that are present in the structure, namely C14-H14···S1 and C10-H10···N2 are not short enough to show up on the surface as red regions. However H···N and H···S contacts constitute 26.9 and 11.2% of the Hirshfeld surface.
Analysis of the surface mapped with shape index function indicates presence of stacking interactions between pirydyl rings and thiazole rings of adjacent molecules (marked on Fig. 8). The most important types of interactions between molecules in the crystal structure of **4** are van der Waals forces (36.1%) as indicated by decomposed fingerprint plots (Fig. S15).

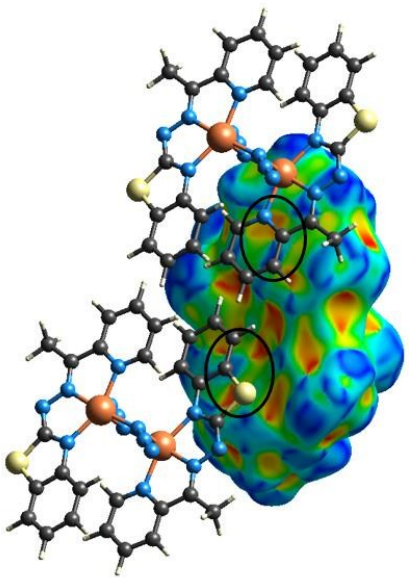

Fig. 8. Hirshfeld surface of **4** mapped with shape index function. Areas marked with ovals represent stacking interactions.

Compound 5

When Hirshfeld surface of **5** is mapped with d_{norm} function several red areas can be noticed. Four large ones correspond to one hydrogen bond, namely N4-H4N···S2 occurring between adjacent complex molecules (Fig. 9a). Most of the other red spots are present due to interactions between ethyl groups of lattice ethanol molecules and complex molecules. These interactions include van der Waals forces (short H···H contacts), C-H···C interactions, and C-H···N hydrogen bonds (Fig. 9b). Additionally there are four small red spots corresponding to C-H···C interactions between adjacent complex molecules. These indicate presence of C-H···π interactions that take part in stacking of molecules in the crystal structure. Mapping of the surface with shape index function reveals that apart from C-H···π interactions, π···π stacking interactions are also present ('bow-tie' patterns marked on Fig. S16). Decomposed fingerprint plots (Fig. S17) indicate that van der Waals forces (47.0%) are a predominant type of interaction in packing of molecules in the structure **5**. Other important interactions are C-H···π stacking (25.6%), π···π stacking (4.7%), and hydrogen bonding – N-H···S (12.0%) and C-H···N (8.0%).

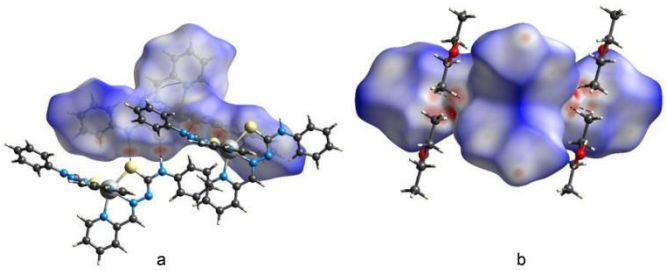

Fig. 9. Hirshfeld surface of **5** mapped with d_{norm} function: a) with N-H···S hydrogen bonds marked as dashed lines; b) with C-H···N interactions markes as dashed lines.

Compound 6

Examination of Hirshfeld surface of **6** mapped with d_{norm} function reveals twelve red areas on the surface (nine of them visible on Fig. 10). Four of them correspond to a N-H···S hydrogen bond (namely N4-H4N···S1) which was observed in the other compounds of this series. In addition molecules of the complex are held together by C-H···π interactions occurring between pirydyl ring of one molecule and phenyl ring of the adjacent one, which are represented on the surface as four small red spots (C3-H3A···C13 contact). The last four of the red areas are associated with C-H···O hydrogen bonding occurring between complex molecules and lattice methanol molecules (C1-H1A···O10 and C6-H6A···O10). There is an additional hydrogen bond in which the oxygen atom of the methanol molecules serves as the donor and N3 atom of the ligand is the acceptor. Appling shape index function to the surface allows to distinguish 'bow-tie' patterns which implicates presence of π···π stacking interactions between pirydyl rings of nearby molecules (Fig. S18). By examining the decomposed fingerprint plots (Fig. S19) it can clearly be seen that apart from van der Waals forces (36.9%) and stacking interactions (32.3%) hydrogen bonds (8.0% of the surface contributed by H···O contacts and 12.9% by H···S contacts) play important role in

molecule stacking in the crystal. Very obvious asymmetry of the fingerprint plots observed for **5** and **6** is due to the fact that lattice ethanol and methanol molecules which are outside of the surface act as donors and acceptors of hydrogen bonds, therefore number of donors and acceptors positioned inside the surface is different to one outside of the surface.

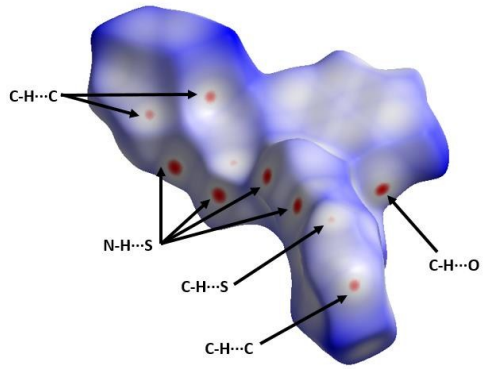

Fig. 10. Hirshfeld surface of **6** mapped with d_{norm} function, with highlighted interaction.

Compound 7

On the Hirshfeld surface of **7** mapped with d_{norm} function seven red areas are visible. Three large ones (Fig. 11) correspond to two classic strong hydrogen bonds between complex molecule and azide ions (N4-H4A···N9 and N8-H8···N11) as well as one weaker interaction (C24-H24···N10). Additionally one can notice four smaller red spots. Two of them are caused by weak C-H···N interactions which also connect complex molecule and the azide ion. The other two red areas indicate presence of C-H···π (H···C contact) interactions between aromatic rings of the complex molecule. When shape index function is applied, one can see red parts of the surface, which indicate C-H···π and C-H···C interactions (marked with arrows on Fig. S20).

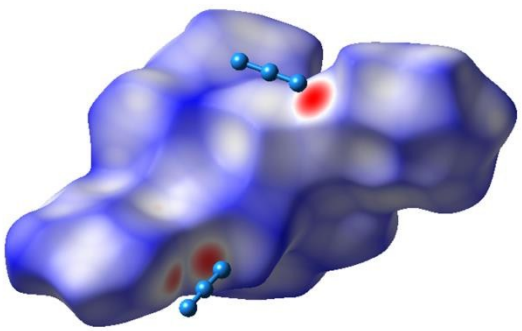

Fig. 11. Hirshfeld surface of **7** mapped with d_{norm} function. Two red larger areas indicate N-H···N hydrogen bond and the smaller one indicates C-H···N interaction.

Examination of decomposed fingerprint plots indicates that van der Waals forces (43.2%), C-H···π interactions (25.2%) and strong hydrogen bonds constitute most of the Hirshfeld surface. Distinct asymmetry of the fingerprint plot (Fig. S21) is caused by the fact that the azide ion positioned outside of the surface serves solely as recipient of hydrogen bonds.

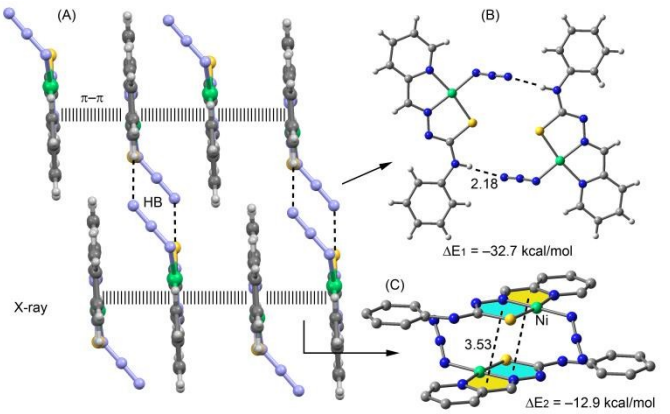

Fig. 12. (A) Partial view of the X-ray solid state structure of **1**. (B, C) Theoretical models used to evaluate the hydrogen bonding and chelate–chelate interactions in complex **1**. Distances are in Å.

3.5 Theoretical study of the supramolecular assemblies

We have focused the theoretical study to analyse the interesting supramolecular assemblies observed in the solid state of complexes **1**–**4** and **7**, focusing our attention to the more unconventional interactions. Particularly, in the Ni compounds **1** and **2** we have analysed the chelate–π interactions. In Fig. 12A it is shown a fragment of the X-ray solid state structure of compound **1** and it can be clearly observed the formation of 1D infinite chains dominated by π-stacking interactions. Each 1D chain interacts with the adjacent one by means of two symmetrically equivalent N–H···N hydrogen bonds forming 2D layers (see Fig 12A and B). A careful inspection of the stacking interaction reveals that it can be better defined as an antiparallel chelate–chelate stacking interaction. To rationalize this issue, we have computed the molecular electrostatic potential (MEP) surface of compound **1** that is represented in Fig. 13A.

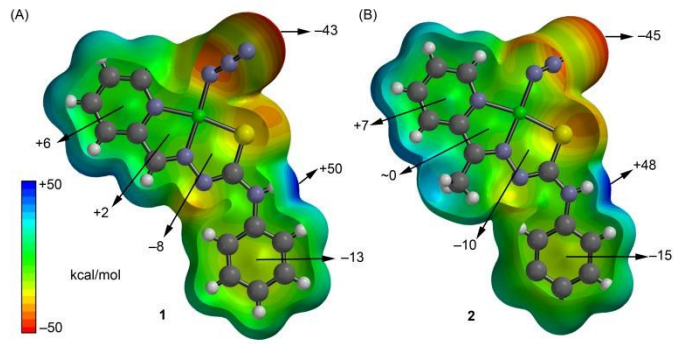

Fig. 13 MEP surfaces of compounds **1** (A) and **2** (B) computed at the B3LYP/6-31+G* level of theory. The MEP values at selected points of the surface are indicated.

Expectedly, the most positive part corresponds to the N–H group and the most negative part to the N_3^- ligand, thus explaining the large interaction energy (ΔE_1 = –32.7 kcal/mol) computed for the H-bonded self-assembled dimer shown in

Figure 12B. More interestingly, the MEP value over the center of the chelate ring containing Sulphur is negative and the MEP value is slightly positive over the other chelate ring, thus favouring the antiparallel arrangement of the stacking complex and also explaining the large chelate-chelate binding energy (ΔE_2 = –12.9 kcal/mol).

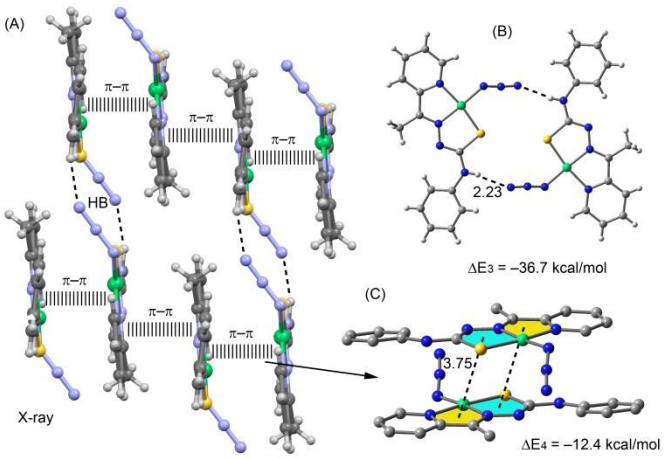

Fig. 14 (A) Partial view of the X-ray solid state structure of **2**. (B, C) Theoretical models used to evaluate the hydrogen bonding and chelate–chelate interactions in complex **2**. Distances are in Å.

Compounds **1** and **2** exhibit similar solid state architectures where chelate–chelate stacking and H-bonding interactions play a prominent role. The main difference is that the chelate rings, which participate in the stacking interactions forming the 1D chains, are more off-set displaced (see Fig. 14) in **2**. The MEP of compound **2** is shown in Fig. 13B and it is very similar to **1**, showing comparable maximum and minimum MEP values at the N–H and azide groups, respectively. Furthermore, the MEP value over the chelate ring that contains the sulphur is more negative in **2** than in **1** and the MEP over the other chelate ring is negligible in **2** likely due to the presence of the methyl group.

The binding energies of the theoretical models used to evaluate the H-bonding and chelate–chelate interactions are given in Fig. 14B and C and they are comparable to those obtained for compound **1**, thus showing that the presence of the methyl group has a little influence on the interaction energies.

In compound **3** we have studied the formation of electrostatically enhanced $\pi^{\delta+}$–$\pi^{\delta-}$ interactions in the solid state (see Fig. 15A). The MEP surface calculated for complex **3** shows that the potential energy value over the pyridine ring that is coordinated to Cu(II) is positive (π-acidic ring, +13 kcal/mol, see Fig. 15B). In contrast the MEP over the phenyl is negative (π-basic ring, –14 kcal/mol). In addition, the chelate ring fused to the pyridine presents a significant positive potential energy (+13 kcal/mol) and the other one presents a small and negative MEP value. Consequently the π-stacking interaction between the pyridine (including the fused chelate ring) and benzene rings is electrostatically favoured. As a matter of fact, the interaction energy of the model dimer (see Fig. 15C) is large and negative ΔE_5 = –16.7 kcal/mol in line with the MEP analysis and the formation of such assemblies in the solid state.

In compound **4** we have examined an interesting chalcogen bonding interaction observed in the solid state. The importance of σ-hole interactions in crystal engineering and other fields has been recently reviewed,[39] including elements of groups IV to VII acting as σ-hole donors and any electron rich entity (lone pair, anion, π-system). In compound **4**, N···S interactions between the azide and the S atom of the five membered ring are present in the solid state (see Fig. 16A). The nitrogen atom is located along the prolongation of the C–S covalent bond, as is common in directional σ-hole bonding, at 3.25 Å that is shorter than the sum of van der Walls radii (3.35 Å). In fact, the MEP surface computed for **4** shows that the potential energy is distributed anisotropically around sulphur. That is, the MEP is

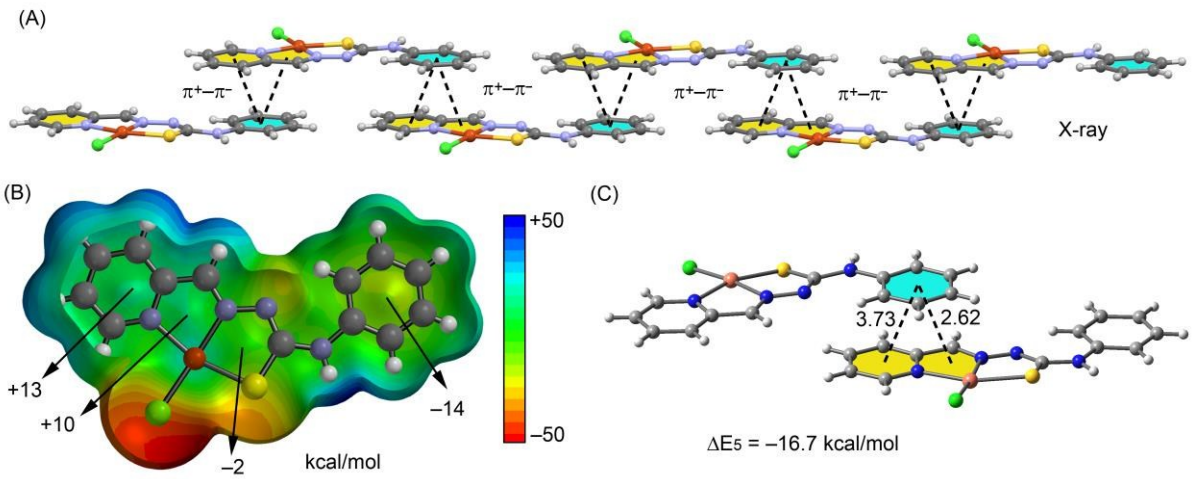

Fig. 15. (A) Partial view of the X-ray solid state structure of **3**. (B) MEP surface of compound **3** at the B3LYP/6-31+G* level of theory. (C) Theoretical model used to evaluate the $\pi^{\delta+}$–$\pi^{\delta-}$ interaction in complex **3**. Distances are in Å.

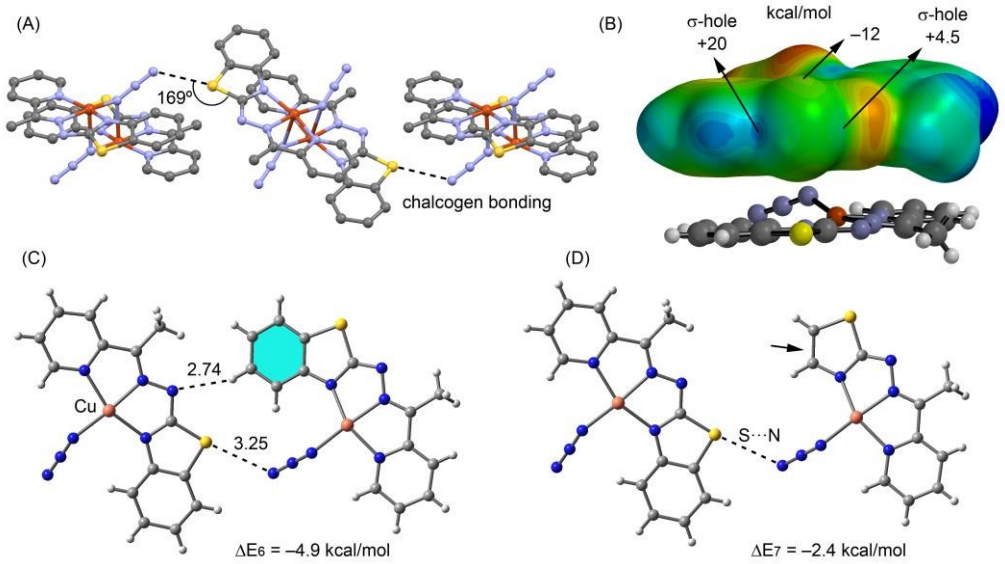

Fig. 16. (A) Partial view of the X-ray solid state structure of **4** (H-atoms omitted for clarity). (B) MEP surface of compound **4** at the B3LYP/6-31+G* level of theory. (C, D) Theoretical model used to evaluate the contribution of the C–H···N and S···N interactions in complex **4**. Distances are in Å.

negative at the lone pairs (–12 kcal/mol) and positive opposite to the S–C covalent bonds (+20 and + 4.5 kcal/mol, see Fig. 16B). We have evaluated the σ-hole interactions using two theoretical models. The first one (see Fig. 16C) is a dimer that has been retrieved from the crystallographic coordinates and the resulting interaction energy is ΔE_6 = –4.9 kcal/mol. In this dimer formation, there is also a contribution of a hydrogen bond established between a nitrogen atom of one ligand and an aromatic C–H bond of the adjacent ligand (see Fig. 16C). Therefore, we have computed an additional theoretical model where one ligand has been simplified eliminating the aromatic ring (see small arrow in Fig 16D). As a result the interaction energy is reduced to ΔE_7 = –2.4 kcal/mol that corresponds to the σ-hole bonding interaction and the difference with respect to ΔE_6 (–2.5 kcal/mol) is the contribution of the N···H–C hydrogen bond. In compound **7** we have also observed a similar chalcogen bonding interaction between the uncoordinated azide anion and the sulfur atom that is further discussed below in the AIM analysis.

Finally, we have used the Bader's theory of "atoms in molecules", which provides an unambiguous definition of chemical bonding, to further describe the noncovalent chelate–chelate ring stacking and chalcogen/hydrogen bonding interactions described above. The AIM theory has been effectively utilized to characterize a great variety of interactions.[40]

In Fig. 17 we show the AIM analysis of the self-assembled dimers of compounds **1** and **2**, which reveals a similar distribution of critical points and bond paths. It can be observed that the chelate-chelate interactions are characterized by the presence of several bond (red spheres), ring (red spheres) and cage (green spheres) critical points (CPs). Basically, two bond CPs connect the sulphur atoms to the carbon atoms of the C=N bond (resembling a π-hole interaction)[39] and another two bond CPs connect the nitrogen atoms to the Ni(II) metal centers.

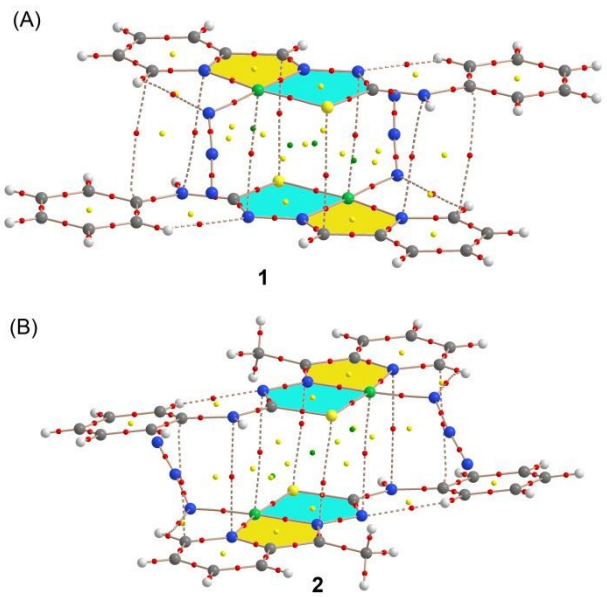

Fig. 17. AIM analyses of complexes **1** and **2**. Bond, ring and cage critical points are represented by red, yellow and green spheres, respectively. The bond paths connecting bond critical points are also represented by dashed lines.

The π–π interaction is further characterized by additional CPs that connect the pyridine ring of one ligand to the Ph–N bond of the other ligand and vice versa. As a consequence of this complicated distribution of bond CPs, several ring and cage CPs are also generated upon complexation due to the formation of supramolecular ring and cages. The value of the Laplacian of the charge density computed at the bond critical points in both

complexes is positive, as is common in closed-shell interactions.

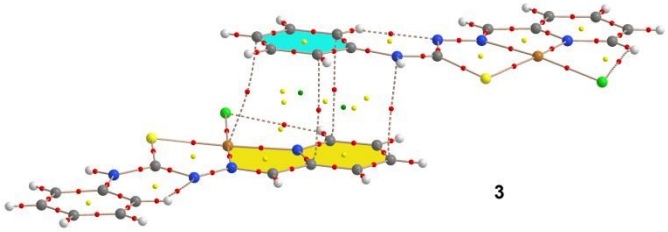

Fig. 18 AIM analysis of complex **3**. Bond, ring and cage critical points are represented by red, yellow and green spheres, respectively. The bond paths connecting bond critical points are also represented by dashed lines.

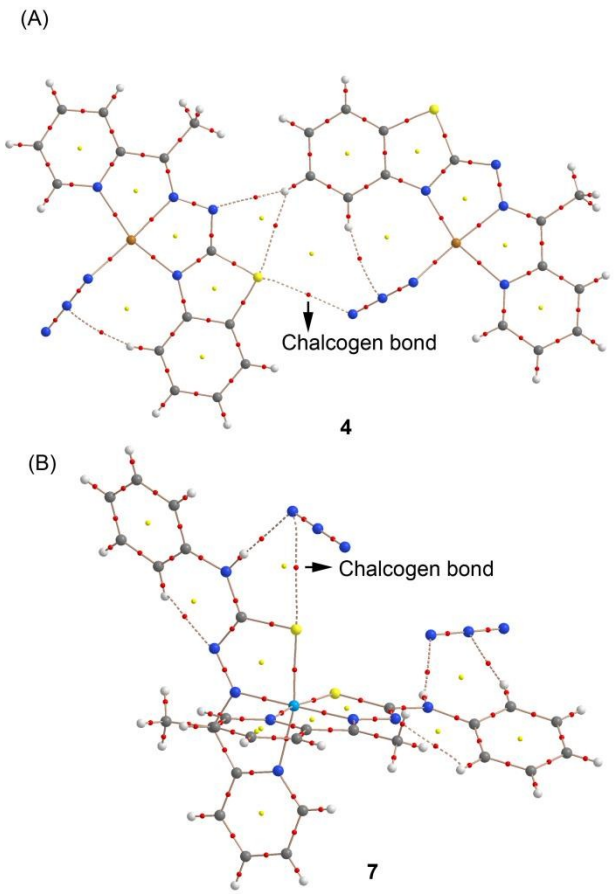

Fig. 19 AIM analyses of complexes **4** and **7**. Bond and ring critical points are represented by red and yellow spheres, respectively. The bond paths connecting bond critical points are also represented by dashed lines.

In Fig. 18 it is shown the AIM analysis of the dimer of compound **3**. It can be observed that the π–stacking interaction is characterized by the presence of several bond (red spheres), ring (red spheres) and cage (green spheres) critical points (CPs). The phenyl ring ($\pi^{\delta-}$) is connected to both the pyridine ($\pi^{\delta+}$) and the chelate ring ($\pi^{\delta+}$). The electron rich and exocyclic nitrogen atom also participates in the stacking interaction since it is connected to the electron poor pyridine ring by means of one bond CP. The each $\pi^{\delta-}$–$\pi^{\delta+}$ interaction is characterized by the presence of four bond, four ring and two cage CPs. The bond paths connect three atoms of phenyl ring and the N atom two three carbon atoms of the coordinated pyridine ring and the Cu atom, thus confirming the existence of the chetale–π interaction in compound **3**.

In Fig. 19 it is shown the AIM analyses of X-ray fragments of compounds **4** and **7** used to characterize the chalcogen interaction. In both compounds the S···N interaction is confirmed by the presence of a bond CP and a bond path connecting one end of azide (either as ligand in **4** or counterion in **7**) to the S atom. In compound **4**, it can be also observed the intermolecular H bonds described above involving the aromatic C–H group as acceptor. Interestingly, it is a bifurcated H–bond where both the N and S atoms participate.

4. Conclusion

In summary, we herein reported the syntheses and structural characterization of seven new metal complexes with two thiosemicarbazone ligands differing only in presence/absence of one methyl group. Interestingly, in the presence of Cu(II) a new ligand is formed (L_3) that comes from an unusual cyclization of the thiosemicarbazone HL_2 catalyzed by the metal center. Compounds **1**–**3** exhibit interesting antiparallel chelate−chelate and chelate–π stacking interactions in the solid state with normal π–π distances that have been studied using DFT calculations. The energies associated to the interactions have been computed using DFT calculations. In general, the chelate–π and chelate−chelate interactions are stronger than that reported for benzene dimer and benzene-chelate complexes. This is due to the higher electrostatic contribution to the π-stacking due to the influence of the metal centers (Ni and Cu) and the antiparallel arrangement of the stacked rings, as shown by the MEP analysis. Our results might be important to understand the solid state architecture of organic–inorganic materials systems that contain metal-chelate rings and organic aromatic molecules.

Acknowledgements

We are grateful to the University of Maragheh for the generous financial support of this research. A.B. and A.F. thank DGICYT of Spain (projects CTQ2014-57393-C2-1-P and CONSOLIDER INGENIO CSD2010–00065, FEDER funds) for funding. We thank the CTI (UIB) for free allocation of computer time.

Notes and references

[a]*Department of Chemistry, Faculty of Science, University of Maragheh, P.O. Box 55181–83111, Maragheh, Iran*
E–mail: mahmoudi_ghodrat@yahoo.co.uk
[b]*Departamento de Química Inorgánica, Facultad de Farmacia, Universidad de Santiago de Compostela, Santiago de Compostela, (Spain)*
[c]*Faculty of Chemistry, Wrocław University of Technology, 27 Wybrzeze Wyspiańskiego Street, 50–370 Wrocław, Poland*

[d]Departamento de Quimica, Universitat de les IllesBalears, Crta. de Valldemossa km 7.5, 07122 Palma de Mallorca (Baleares), Spain; E–mail: toni.frontera@uib.es
[e]UCSD Crystallography Facility, Department of Chemistry and Biochemistry, University of California, San Diego, 9500 Gilman Drive, La Jolla, USA
[f]Instutute of Low Temperature and Structure Research, Polish Academy of Sciences, Okólna 2, 50-422 Wrocław, Poland

† CCDC 1046009-1046016 contain the supplementary crystallographic data for this paper. These data can be obtained free of charge from The Cambridge Crystallographic Data Centre via www.ccdc.cam.ac.uk/data_request/cif.

Electronic Supplementary Information (ESI) available: [details of any supplementary information available should be included here]. See DOI: 10.1039/b000000x/

1 a) D. R. Richardson, *Crit. Rev. Oncol. Hematol*., 2002, **42**, 267; b) P. Jutten, W. Schumann, A. Hartl, L. Heinisch, U. Grafe, W. Werner and H. Ulbricht, *Bioorg. Med. Chem. Lett*., 2002, **12**, 1339; c) J. S. Casas, M. S. García-Tasende and J. Sordo, *Coord. Chem. Rev*., 2000, **209**, 197–261; d) T. S. Lobana, R. Sharma, G. Bawa and S. Khanna, *Coord. Chem. Rev*., 2009, **253**, 977–1055; c) A. Basu and G. Das, *Inorg. Chim. Acta*., 2011, **372**, 394–399.

2 a) A. G. Quiroga and C. Navarro-Ranninger, *Coord. Chem. Rev*., 2004, **248**, 119–133; b) C. Q. Debra, A. K. Kathy and R. K. Earl, *Antiviral Res*., 2006, **71**, 24–30; c) W. F. T. McMath and H. T. H. Wilson, *Br Med. J*., 1956, **1**, 1041–1042; d) A. M. Tsimberidou, Y. Alvarado and F. J. Giles, *Expert Rev Anticancer Ther*, 2002, **2**, 437–448; e) M. C. R. Arguelles, E. C. L. Silva, J. Sanmartín, P. Pelagatti and F. Zani, *J. Inorg. Biochem*., 2005, **99**, 2231–2239; f) R. Prabhakaran, V. Krishnan, K. Pasumpon, D. Sukanya, E. Wendel, C. Jayabalakrishnan, H. Bertagnolli and K. Natarajan, *Appl. Organomet. Chem*., 2006, **20**, 203–213; g) R. Prabhakaran, R. Huang, R. Karvembu, C. Jayabalakrishnan and K. Natarajan, *Inorg. Chim. Acta*, 2007, **360**, 691–694; h) R. Prabhakaran, R. Huang, S. V. Renukadevi, R. Karvembu, M. Zeller and K.Natarajan, *Inorg. Chim. Acta*, 2008, **361**, 2547–2552; i) Prabhakaran, S. Anantharaman, M. Thilagavathi, M. V. Kaveri, P. Kalaivani, R. Karvembu, N. Dharmaraj, H. Bertagnolli and K. Natarajan, *Spectrochim. Acta, Part A*, 2011, **78**, 844–853; j) R. Prabhakaran, P. Kalaivani, R. Jayakumar, M. Zeller, A. D. Hunter, S. V. Renukadevi, E. Ramachandran and K. Natarajan, *Metallomics*, 2011, **3**, 42–48; k) R. Prabhakaran, P. Kalaivani, R. Huang, M. Sieger, W. Kaim, P. Viswanathamurthi, F. Dallemer and K. Natarajan, *Inorg. Chim. Acta*, 2011, **376**, 317–324; l) P. Kalaivani, R. Prabhakaran, E. Ramachandran, F. Dallemer, G. Paramaguru, R. Renganathan, P. Poornima, V. V. Padma and K. Natarajan, *Dalton Trans.*, 2012, **41**, 2486–2499; m) R. Prabhakaran, P. Kalaivani, P. Poornima, F. Dallemer, G. Paramaguru, V. Vijaya Padma, R. Renganathan, R. Huange and K. Natarajan, *Dalton Trans*., 2012, **41**, 9323–9336; n) M. C. R. Arguelles, E. C. L. Silva, J. Sanmart|n, A. Bacchi, C. Pelizzi and F. Zani, *Inorg. Chim.Acta*, 2004, **357**, 2543–255; o) A. Cukurovali, I. Yilmaz, S. Gur and C. Kazaz, *Eur. J. Med. Chem.*, 2006, **41**, 201–207; p) W. X. Hu, W. Zhou, C. Xia and X. Wen, *Bioorg. Med. Chem. Lett*., 2006, **16**, 2213–2218; q) Z. Afrasiabi, E. Sinn, S. Padhye, S. Dutta, S. Padhye, C. Newton, C. E. Anson and A. K. Powell, *J. Inorg. Biochem*., 2003, **95**, 306–314; r) T. Bal, B. Atasever, Z. Solakoglu, S. E. Kuruca and B. Ulkuseven, *Eur. J. Med. Chem.*, 2007, **42**, 161–167.

3 a) E. W. Ainscough, E. N. Baker, A. M. Brodie, R. J. Cresswell, J. D. Ranford and J. M. Waters, *Inorg. Chim. Acta*, 1990, **172**, 185-190; b) E. W. Ainscough, A. M. Brodie, J. D. Ranford and J. M. Waters, *J. Chem. Soc., Dalton Trans*., 1991, 1737-1742; c) J. García-Tojal, J. García-Jaca, R. Cortés, T. Rojo, M. K. Urtiaga and M. I. Arriortua, I*norg. Chim. Acta*, 1996, **249**, 25-32; d) P. Gómez-Saiz, J. García-Tojal, M. Maestro, J. Mahía, L. Lezama and T. Rojo, *Eur. J. Inorg. Chem*., 2003, 2123-2132.; e) B. García, J. García-Tojal, R. Ruiz, R. Gil-García, S. Ibeas, B. Donnadieu and J. M. Leal, *J. Inorg. Biochem*., 2008, **102**, 1892.

4 a) C. F. Bell and C. R. Theocharis, *Acta Crystallogr., Sect. C: Cryst. Struct. Commun.*, 1987, **43**, 26; b) A. G. Bingham, H. Bogge, A. Muller, E. W. Ainscough and A. M. Brodie, *J. Chem. Soc., Dalton Trans.*, 1987, 493; c) J. García-Tojal, M.K. Urtiaga, R. Cortes, L. Lezama, M. I. Arriortua and T. Rojo, *J. Chem. Soc., Dalton Trans.* 1994, 2233; d) E.W. Ainscough, A.M. Brodie, J.D. Ranford and J. M. Waters, *J. Chem. Soc., Dalton Trans.* 1997, 1251; e) P. Gómez-Saiz, J. García-Tojal, M. A. Maestro, F. J. Arnáiz and T. Rojo, *Inorg. Chem.*, 2002, **41**, 1345; f) P. Gómez-Saiz, J. García-Tojal, M. A. Maestro, J. Mahía, F.J. Arnáiz, L. Lezama and T. Rojo, *Eur. J. Inorg. Chem.*, 2003, 2639; g) P. Gómez-Saiz, J. García-Tojal, A. Mendía, B. Donnadieu, L. Lezama, J. L. Pizarro, M. I. Arriortua and T. Rojo, *Eur. J. Inorg. Chem.*, 2003, 518; h) P. Gómez-Saiz, R. Gil-García, M. A. Maestro, J. L. Pizarro, M. I. Arriortua, L. Lezama, T. Rojo and J. García-Tojal, *Eur. J. Inorg. Chem.*, 2005, 3409; i) E. W. Ainscough, A. M. Brodie, J. D. Ranford and J. M. Waters, *J. Chem. Soc., Dalton Trans.*, 1991, 2125; j) J. García-Tojal, L. Lezama, J.L. Pizarro, M. Insausti, M.I. Arriortua and T. Rojo, *Polyhedron*, 1999, **18**, 3703; k) P. Gómez-Saiz, R. Gil-García, M. A. Maestro, J.L. Pizarro, M.I. Arriortua, L. Lezama, T. Rojo, M. González-Álvarez, J. Borrás and J. García-Tojal, *J. Inorg. Biochem., 2008*, **102**, 1910.

5 a) Y. M. Chumakov, V. I. Tsapkov, E. Jeanneau, N. N. Bairac, G. Bocelli, D. Poirier, J. Rou and A. P. Gulea, *Crystallogr. Rep.*, 2008, 786; b) R. Gil-García, R. Zichner, V. Díez-Gómez, B. Donnadieu, G. Madariaga, M. Insausti, L. Lezama, P. Vitoria, M. R. Pedrosa and J. García-Tojal, *Eur. J. Inorg. Chem.*, 2010, 4513.

6 a) J. Sponer, K. E. Riley and P. Hobza, *Phys. Chem. Chem. Phys.*, 2008, **10**, 2595–2610; b) X. J. Wang, L. C. Gui, Q. L. Ni, Y. F. Liao, X. F. Jiang, L. H. Tang, L. H. Zhang and Q. Wu, *CrystEngComm*, 2008, **10**, 1003–1010; c) S. L. Cockroft, C. A. Hunter, K. R. Lawson, J. Perkins and C. J. J. Urch, *J. Am. Chem. Soc.*, 2005, **127**, 8594–8595; d) T. Sato, T.Tsuneda and K. Hirao, *J. Chem. Phys.*, 2005, **123**, 104307; e) S. Grimme, *Angew. Chem., Int. Ed.*, 2008, **47**, 3430–3434; f) E. C. Lee, D. Kim, P. Jurecka, P. Tarakeshwar, P. Hobza and K. S. Kim, *J. Phys. Chem. A*, 2007, **111**, 3446–3457; g) M. O. Sinnokrot and C. D. Sherrill, *J. Phys. Chem. A*, 2006, **110**, 10656–10668; h) M. Pitonak, P. Neogrady, J. Rezac, P. Jurecka, M. Urban and P. Hobza, *J. Chem. Theory Comput.*, 2008, **4**, 1829–1834.

7 a) B. D. Ostojić, G. V. Janjić, S. D. Zarić, *Chem. Commun.*, 2008, **48**, 6546–6548; b) Z. D. Tomić, S. B. Novaković and S. D. Zarić, *Eur. J. Inorg. Chem.*, 2004, **11**, 2215–2218; c) D. N. Sredojević, Z. D. Tomić and S. D. Zarić, Cent. *Eur. J. Chem.*, 2007, **5**, 20–31; d) Z. D. Tomić, D. N. Sredojević and S. D. Zarić, *Cryst. Growth Des.*, 2006, **6** 29–31; e) D. N. Sredojević, G. A. Bogdanović, Z. D. Tomić and S. D. Zarić, *CrystEngComm*, 2007, **9,** 793–798; e) E. Craven, C. Zhang, C.

Janiak, G. Rheinwald and H. Z. Lang, *Anorg. Allg. Chem.*, 2003, **629** 2282–2290; f) U. Mukhopadhyay, D. Choquesillo-Lazarte, J. Niclos-Gutierrez and I. Bernal, *CrystEngComm*, 2004, **6**, 627–632; g) D. Pucci, V. Albertini, R. Bloise, A. Bellusci, A. Cataldi, C. V. Catapano, M. Ghedini, A. J. Crispini, *Inorg. Biochem.*, 2006, **100** 1575–1578; h) S. P. Mosae, E. Suresh and P. S. Subramanian, Polyhedron, 2009, **28**, 245–252; i) X. J. Wang, H. X. Jian, Z. P. Liu, Q. L. Ni, L. C. Gui and L. H. Tang, *Polyhedron*, 2008, **27**, 2634–2642; j) S. Chowdhury, M. G. B. Drew and D. Datta, *Inorg. Chem. Commun.*, 2003, **6**, 1014–1016; k) X. Wang, O. V. Sarycheva, B. D. Koivisto, A. H. Mckie and F. Hof, *Org. Lett.* 2008, **10**, 297–300.

8 E. Bermejo, A. Castineiras, R. Dominguez, R. Carballo, C. Maichle-Moessmer, J. Straehle and D.X. West, *Z. Anorg. Allg. Chem.*, 1999, **625**, 961-968.

9 APEX2 Software, Bruker AXS Inc., v2014.71, Madison, Wisconsin, USA, 2014.

10 Oxford Diffraction (2006). CrysAlis CCD. Oxford Diffraction Ltd, Abingdon, Oxfordshire, England.

11 G. M. Sheldrick, SADABS. Program for Empirical Absorption Correction of Area Detector Data. University of Göttingen, Germany, 2001.

12 G. M. Sheldrick, *Acta Crystallogr.* 2015, **A71**, 3-8.

13 L. J. Farrugia, *J. Appl. Cryst.* 2012, **45**, 849-854.

14 K. Brandenburg and H. Putz, Diamond, version 3.2, Crystal Impact GbR: Bonn, Germany, 2009.

15 R. Ahlrichs, M. Bär, M. Häser, H. Horn and C. Kölmel, *Chem. Phys. Lett.*, 1989, **162**, 165.

16 S. F. Boys and F. Bernardi, *Mol. Phys.*, 1970, **19**, 553–566.

17 R. F. W. Bader, *Chem. Rev.*, 1991, **91**, 893–928.

18 T. A. Keith, AIMAll (Version 13.05.06), TK Gristmill Software, Overland Park KS, USA, 2013.

19 a) S. Roy, A. Bauza, A. Frontera, F. Schaper, R. Banik, A. Purkayastha, B. M. Reddy, B. Sridhar, M. G. B. Drew, S. Kr Das and S. Das, *Inorg. Chim. Acta*, 2016, **440**, 38-47; b) G. Mahmoudi, A. Bauzá, A. Rodríguez-Diéguez, P. Garczarek, W. Kaminsky and A. Frontera, *CrystEngComm*, 2016, **18**, 102-112; c) A. Bauzá, T. J. Mooibroek and A Frontera, *CrystEngComm*, 2016, **18**, 10-23; M. Abedi, O. Z. Yeşilel, G. Mahmoudi, A. Bauzá, S. E. Lofland, Y. Yerli, W. Kaminsky, P. Garczarek, J. K. Zaręba, A. Ienco, A. Frontera and M. S. Gargari, *Inorg. Chim. Acta*, 2016, DOI d) M. Roy, A. Bauzá, A. Frontera, S. Banerjee, S. Halder and A. Saha, *Polyhedron*, 2015, **102**, 764-772; e) Y. Lagos, J. Palou-Mir, A. Bauzá, J. J. Fiol, Á. García-Raso, À. Terrón, E. Molins, M. Barceló-Oliver and A. Frontera, *Polyhedron*, 2015, **102**, 735-740

20 S. K. Wolff, D. J. Grimwood, J. J. McKinnon, M. J. Turner, D. Jayatilaka and M. A. Spackman, Crystal Explorer ver. 3.1, University of Western Australia, Perth, Australia, 2013.

21 a) V. Philip, V. Suni, M. R. P. Kurup and M. Nethaji, *Polyhedron*, 2004, **23**, 1225–1233; b) A. Panja, D. M. Eichhorn, *Inorg. Chim. Acta* 2012, **391**, 88–92; c) B. Shaabani, A. A. Khandar, M. Dusek, M. Pojarova, M. A. Maestro, R. Mukherjee and F. Mahmoudi, *J. Coord. Chem.* 2014, **67**, 2096-2109.

22 a) J. A. Less, D. C. Reis, I. C. Mendes, N. L. Speziali, L. F. Rocha, V. R.A. Pereira, C. M.L. Melo, H. Beraldo, *Polyhedron*, 2011, **30**, 372–380; b) A. Basu, D. Thiyagarajan, C. Kar, A. Ramesh, G. Das, *RSC Adv.*, 2013, **3**, 14088–14098; c) D. Kovala-Demertzi, V. Varagi, M. A. Demertzis, C. P. Raptopoulou and A. Terzis, *Acta Crystallogr.* 1996, **C52**, 2027-2029; d) M. A. Soares, J. A. Lessa, I. C. Mendes, J. G. Da Silva, R. G. dos Santos, L. B. Salum, H. Daghestani, A. D. Andricopulo, B. W. Day, A. Vogt, J. L. Pesquero, W. R. Rocha and H. Beraldo, *Bioorg. Med. Chem.* 2012, **20**, 3396–3409.

23 a) C. Janiak, *J. Chem. Soc., Dalton Trans.*, 2000, 3885–3896; b) A. Castiñeiras, A. G. Sicilia-Zafra, J. M. González-Pérez, D. Choquesillo-Lazarte and J. Niclós-Gutiérrez, *Inorg. Chem.* 2002, **41**, 6956-6958.

24 L. Yang, D. R. Powell and R. P. Houser, *Dalton Trans.*, 2007, 955-964.

25 A. W. Addison, T. N. Rao, J. Reedijk, J.van Rijn and G. C. Verschoor, *J. Chem. Soc., Dalton Trans.* 1984, 1349.

26 a) M. C. Aguirre, J. Borrás, A. Castiñeiras, J. M. García-Monteagudo, I. García-Santos, J. Niclós and D. X. West, *Eur. J. Inorg. Chem.* 2006, 1231–1244; b) A. B. Beshir, S. K. Guchhait, J. A. Gascon and G. Fenteany, *Bioorg. Med. Chem. Lett.* 2008, **18**, 498-504

27 E. Gyepes, T. Głowiak and D. Mikloš, *J. Chem. Crystallogr.*, 2000, **30**, 505-507.

28 D. N. Sredojević, Z. D. Tomić and S. D. Zarić, *Cent. Eur. J. Chem.*, 2007, **5**, 20-31.

29 A. Castiñeiras, I. García-Santos, S. Dehnen and P. Sevillano, *Polyhedron* 2006, **25**, 3653–3660.

30 W.-B. Shi, A.-L. Cui and H.-Z. Kou, *Cryst. Growth. Des.*, 2012, **12**, 3436-3443.

31 a) R. J. Kunnath, M. R. P. Kurup and S. W. Ng, *Acta Crystallogr.*, 2012, **E68**, m1195; b) V. Philip, V. Suni, M. R. P. Kurup and M. Nethaji, *Polyhedron*, 2005, **24**, 1133–1142.

32 a) Rajnikant, Dinesh, Kamni, M.B. Deshmukh, S.S. Jagpat and S.R. Desai, *J. Chem. Crystallogr.*, 2005, **35**, 293-296; b) H. R. Lawrence, Z. Li, M. L. R. Yip, S.-S. Sung, N. J. Lawrence, M. L. McLaughlin, G. J. McManus, M. J. Zaworotko, S. M. Sebti, J. Chen and W. C. Guida, *Bioorg. Med. Chem. Lett.* 2009, **19**, 3756–3759; c) H.-K. Fun, Ch. K. Quah, D. Munirajasekhar, M. Himaja and B. K. Sarojini, *Acta Crystallogr.* 2012, **E68**, o2438–o2439.

33 M. R. Bermejo, A. M. González-Noya, M. Martínez-Calvo, R. Pedrido, M. Maneiro, M. I. Fernández and E. Gómez-Fórneas, *Z. Anorg. Allg. Chem.* 2007, **633**, 1911-1918.

34 a) A. Usman, I. A. Razak, S. Chantrapromma, H.-K. Fun, A. Sreekanth, S. Sivakumarb and M. R. P. Kurup, *Acta Crystallogr.* 2002, **C58**, m461-m463; b) M. R. Bermejo, A. M. González-Noya, M. Martínez-Calvo, R. Pedrido, M. J. Romero, M. I. Fernández and M. Maneiro, *Z. Anorg. Allg. Chem.* 2007, **633**, 807-813.

35 D. Kovala-Demertzi, U. Gangadharmath, M. A. Demertzis and Y. Sanakis, *Inorg. Chem. Commun.* 2005, **8**, 619–622.

36 A. de Souza Fonseca, V. Carratu Gervini, L. Bresolin, A. Locatelli, and A. Bof de Oliveira, *Acta Crystallogr.* 2012, **E68**, m635–m636.

37 a) D. X. West, M. A. Lockwood and A. Castiñeiras, *Transition Met. Chem.*, 1997, **22**, 447-452; b) P. F. Rapheal, E. Manoj, M. R. P. Kurup and E. Suresh, *Polyhedron* 2007, **26**, 607–616.

38 M. A. Spackman and D. Jayatilaka, *CrystEngComm*, 2009, **11**, 19-32.

39 A. Bauzá, T. J. Mooibroek and A. Frontera, *ChemPhysChem*, 2015, **16**, 2496-2517.

40 (a) A. Bauzá and A. Frontera, *ChemPhysChem*, 2015, **16**, 3108-3113; (b) A. Bauzá, A. Frontera, *ChemPhysChem*, 2015, **16**, 3625–3630; (c) A. Bauzá and A. Frontera, *Phys. Chem. Chem. Phys*., 2015, **17**, 24748-24753; (d) E. C. Escudero-Adán, A. Bauzá, A. Frontera and P. Ballester, *ChemPhysChem*, 2015, **16**, 2530-2533; (e) M. Mirzaei, M. Nikpour, A. Bauza and A. Frontera, *ChemPhysChem*, 2015, **16,** 2260-2266; (f) A. Bauzá and A. Frontera, *Chem. Phys. Lett.*, 2015, **633**, 282-286; (g) A. Bauzá and A. Frontera, *Angew. Chem. Int. Ed.*, 2015, **54**, 7340–7343.